Clay Minerals (2019), **54**, 245–254
doi:10.1180/clm.2019.30

CAMBRIDGE UNIVERSITY PRESS

Article

Mineralogical and crystal-chemical characterization of the talc ore deposit of Minzanzala, Gabon

Mathilde Poirier[1]*, Jean-Eudes Boulingui[2,3], François Martin[1], Michel Mbina Mounguengui[4], Charles Nkoumbou[5], Fabien Thomas[3], Michel Cathelineau[6] and Jacques Yvon[5]

[1]Laboratoire Géosciences Environnement Toulouse UMR 5563, UPS-CNRS-IRD-CNES, ERT 1074 'Géomatériaux', 14 Avenue Edouard Belin, 31400 Toulouse, France; [2]Laboratoire des Sciences de la Vie et de la Terre, Ecole Normale Supérieure, B.P. 17009 Libreville, Gabon; [3]Laboratoire Interdisciplinaire des Environnements Continentaux UMR CNRS7360, Université de Lorraine, 15 Avenue du Charmois, B.P. 40, 54501 Vandoeuvre-lès-Nancy, France; [4]Faculté des Sciences de l'Université des Sciences et Techniques de Masuku, USTM B.P. 943 Franceville, Gabon; [5]Département des Sciences de la Terre, Université de Yaoundé I, Faculté des Sciences, B.P. 812 Yaoundé, Cameroon; and [6]Laboratoire GeoRessources UMR CNRS7359, Université de Lorraine, Rue du Doyen Roubault B.P. 40, 54501 Vandoeuvre-lès-Nancy, France

Abstract

This research aims to characterize the mineralogical and crystal-chemical purity of two samples of natural talc (BTT6, BTT7) from the occurrence 'Ecole1' in the deposit of Minzanzala, southwest Gabon. X-ray diffraction and modal-composition calculations demonstrated the presence of quartz and Al–Fe-bearing phases (kaolinite and/or chlorite and/or Al–Fe oxyhydroxides) as accessory minerals in both ores. In contrast, the chemical and spectroscopic characterization of the talc component revealed remarkable chemical purity expressed by very low Fe contents. According to these results, the talc of Minzanzala might be used as a filler in a wide range of industrial applications, such as in cosmetics, paints, polymers or ceramics.

Keywords: crystal-chemistry, Gabon, mineralogy, talc, Tchibanga

(Received 11 July 2018; accepted 18 April 2019; Accepted Manuscript online: 20 June 2019; Associate Editor: Lawrence Warr)

Talc is a magnesium sheet silicate that is valued for its low price, lamellar structure, softness, biocompatibility, thermal stability and chemical inertness, making it a material of choice for many industrial applications (Dumas, 2013). Talc is largely used as a filler in paper industry (Chauhan & Bhardwaj, 2017) and ceramics (Chandra *et al.*, 2004), as a thickener or viscosity enhancer in paints and coatings (Tothill *et al.*, 1993), as a stabilizer in polymers (Kocic *et al.*, 2012), as an additive in agri-food (Mallet *et al.*, 2005) and cosmetics (Zazenski *et al.*, 1995; López-Galindo *et al.*, 2007; Carretero & Pozo, 2010) and as a pleurodesis agent in medicine (Viallat & Boutin, 1998; Maskell *et al.*, 2004).

In 1948, prospecting campaigns led to the discovery of steatite, a rock mainly composed of talc, near the city of Tchibanga in southwest Gabon (Lissoulour & Barras, 1948). Thereafter, large volumes of talc were discovered in the same region all around the Nyanga syncline (Bellivier, 1977; Boutin, 1985; Boutin *et al.*, 2001; Martini & Makanga, 2001). The possible commercial value of the deposit needs to be determined. To this end, the following questions need to be answered: (1) What kinds of minerals are associated with the talc crystals and in what proportions (in order to determine whether mining of the talc deposit is commercially viable)? (2) What is the chemical composition of the talc mineral itself (in order to determine whether or not chemical substitutions in the crystal lattice are present)? The answers to these questions are indeed essential to determining the potential industrial application domains of the present ore (Dumas *et al.*, 2015). For example, a talc containing some Al, Fe or Ca due to the presence of hydrophilic minerals (chlorite and carbonates) will be used preferably in polar media, whereas a purer talc is more hydrophobic and can be used in non-polar media as polyolefins or in cordierite-based ceramics.

This research aimed to characterize the mineralogy and crystal-chemistry of the talc ore of the Minzanzala area in the southwest part of the Nyanga syncline, Gabon. Its characterization will permit the investigation of its potential applications.

Geological setting

The talc ore deposit of Minzanzala is located in southwest Gabon, near the city of Tchibanga (latitude 02°90′487″S, longitude 10°99′161″E). It is part of the large Nyanga syncline, which corresponds to the northern extremity of a Precambrian sedimentary basin extending from Angola to Gabon. The talc mineralization is included in the upper part of a calc-schist formation and is covered by a lateritic layer that is >600 km long and from one to several kilometres wide (Fig. 1).

Sampling

Two different talc samples were recovered from the slopes of Minzanzala in a massive outcrop made of fine sands and clays

*E-mail: mathilde.l.poirier@gmail.com

Cite this article: Poirier M, Boulingui J-E, Martin F, Mbina Mounguengui M, Nkoumbou C, Thomas F, Cathelineau M, Yvon J (2019). Mineralogical and crystal-chemical characterization of the talc ore deposit of Minzanzala, Gabon. *Clay Minerals* **54**, 245–254. https://doi.org/10.1180/clm.2019.30

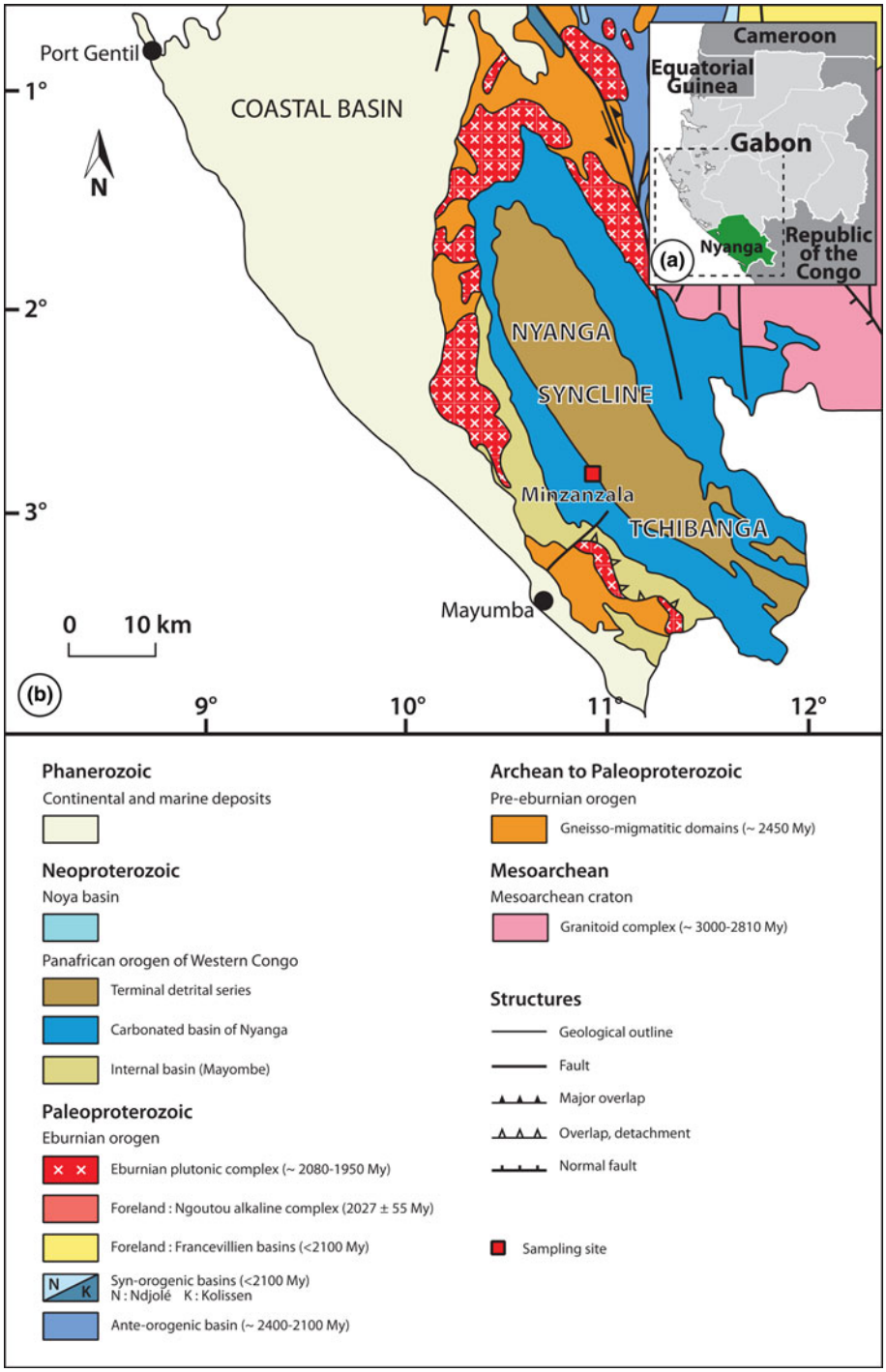

Fig. 1. (a) Location of the study area. (b) Geological map showing the Minzanzala talc deposit.

(Fig. 2). The outcrop was stripped with a hand shovel to obtain an unaltered surface. This surface had white to yellowish colouration, and two blocks were extracted from the core of the unaltered zones to collect the samples. They are referred to as BTT6 (yellowish) and BTT7 (whitish). The samples were then crushed, ground and sieved to three powder fractions (<50, <250 and <500 μm).

Another natural talc, known as Luzenac talc, from the French quarry of Trimouns in the Pyrenees, was used for comparison (donated by Imerys). This talc was received as a finely ground white powder and was selected for its high crystal order and low Fe content (0.68 wt.% Fe_2O_3; Martin *et al.*, 2006).

Methods

X-ray diffraction (XRD) analysis was performed on random talc powders at the LIEC laboratory (Laboratoire Interdisciplinaire des Environnements Continentaux) of Nancy (France) with a Jobin-Yvon Sigma 2080 diffractometer using Co-$K\alpha_1$ radiation ($\lambda = 1.789$ Å). The fraction finer than 250 μm was selected for the analysis. The XRD traces were recorded over the 0–60°2θ range, with a step size of 0.034608°2θ and a count time per step of 0.32 s. Indexation of the XRD peaks was performed with the 'Powder Diffraction File' available from the International Center

https://doi.org/10.1180/clm.2019.30 Published online by Cambridge University Press

Fig. 2. View of the talc outcrop.

for Diffraction Data (ICDD) website. The XRD measurements were also performed on a finer size fraction to avoid a preferential orientation of the talc particles, which might mask mineral impurities in the samples. The initial powders (<500 μm) were ground to 40 μm for BTT6 and 20 μm for BTT7 for 90 min at 25 Hz, using a MM200 mixer mill. The particle size was controlled by laser diffraction using a Beckman Coulter LS100Q device and the *LS32* software. Four measurements were registered and averaged for each sample. The XRD traces of the finely ground samples were recorded at the GET laboratory (Géosciences Environnement Toulouse, France) with a Bruker D2 Phaser diffractometer using Cu-$K\alpha_{1+2}$ radiation over the 0–80°2θ range, with a step size of 0.02°2θ and a count time per step of 0.5 s.

Modal-composition calculations were performed in order to determine the abundance of each phase in both samples. These calculations are based on the mineralogy obtained by XRD and on the whole-rock chemical analysis. On this basis, the modal compositions of the samples may be calculated by using the multilinear method described by Njopwouo (1984) and Yvon *et al.* (1990) by means of the following formula:

$$T(a) = \sum_1^n Mi \times Pi(a)$$

where $T(a)$ represents the content (%) of the chemical element 'a' in the rock; *Mi* represents the content (%) of the mineral '*i*' in the rock and $Pi(a)$ represents the proportion of the element '*a*' in the mineral '*i*'. Only theoretical mineral compositions were used for the calculations, as the chemical compositions of each phase were not available. MgO was assigned to talc (major phase), the remaining SiO_2 was assigned to quartz (second major phase) and the small amounts of Al_2O_3 and FeO were allocated to Al–Fe-bearing phases (kaolinite, chlorite, Al–Fe oxyhydroxides). The MgO and SiO_2 contents of talc and quartz were adjusted accordingly. Kaolinite, chlorite and Al–Fe oxyhydroxides were included in the same 'Al–Fe-bearing phases' group because of the limitations of XRD in terms of separating these phases.

Whole-rock chemical analysis was performed at the CRPG laboratory (Centre de Recherches Pétrographiques et Géochimiques) of Nancy (France) to quantify the major and trace elements in the finer fraction of the samples (<250 μm). The preparation involved alkali fusion followed by HNO_3 acid etching to dissolve the glass obtained. The major elements were quantified using an inductively coupled plasma atomic emission spectrometer coupled with a Jobin-Yvon 70-P quantometer and trace elements were determined by an inductively coupled plasma mass spectrometer coupled with a Perkin Elmer Elan 500 instrument.

Quantitative chemical analyses were performed on the talc particles (<500 μm fraction) using a CAMECA SXFive electron microprobe at the Centre de MicroCaractérisation Raimond Castaing of Toulouse (France) with a 15 kV acceleration voltage, a 10 nA sample current and a defocused beam with a diameter of 2 μm. Talc powders were compressed into pellets with a hand-operated press and their structural formula was calculated based on 22 oxygen atoms. Natural and synthetic minerals were used as standards for calibration (Si: wollastonite; Mg: periclase; Fe: hematite; Al: corundum; Cl: tugtupite; Na: albite; Ca: wollastonite; F: topaz). The Si occupancy was systematically higher than the ideal 8, possibly because of the layer structure of talc coupled with the enrichment in Si during the analysis due to the migration of other elements (Müller *et al.*, 2005). This explanation was favoured because the analyses were only focused on large talc platelets, excluding the presence of quartz admixtures.

Near-infrared (NIR) spectroscopy was performed on talc powders using a Thermo Nicolet Fourier-transform infrared spectrometer (ICT laboratory, Institut de Chimie de Toulouse, France) equipped with a smart NIR integrating sphere (IngaAs detector). Diffuse reflection spectra were recorded between 4000 and 10,000 cm^{-1} at a resolution of 4 cm^{-1} representing the average of 32 scans. The <500 μm fraction was ground in an agate mortar and the powders were placed without further treatment.

^{29}Si and ^{1}H solid-state nuclear magnetic resonance (NMR) spectra were recorded on a Bruker Avance III 400 NMR spectrometer at the LCC laboratory (Laboratoire de Chimie de Coordination, Toulouse, France). All of the samples were spun at 8 kHz at the magic angle using ZrO_2 rotors. For ^{29}Si magic angle spinning (MAS) NMR experiments, a 4 mm probe was used operating at 79.39 MHz. The spectra were recorded under high-power proton decoupling conditions using a small flip angle of 30° and a long recycle delay of 60 s. For the ^{1}H MAS-NMR experiments, a 4 mm probe was employed, operating at 399.60 MHz. The spectra were obtained using a small flip angle of 30° and a recycle delay of 5 s. All of the chemical shifts were referenced externally to tetramethylsilane.

Scanning electron microscopy (SEM) was performed in the SCMEM department (Service Commun de Microscopies Electroniques et de Microanalyses, Nancy, France) using an Hitachi FEG S-4800 apparatus equipped with an energy-dispersive spectrometer (Si-Li Thermo-Noran equipment) and a backscattered electron detector. The SEM images were recorded on carbon-coated <50 μm fractions using a 15 kV acceleration voltage. Double-faced graphite tape was used as an adhesive.

Colorimetric measurement analyses were recorded on the <500 μm fraction with a Minolta 3700d spectrocolorimeter (Imerys, Toulouse, France). A D65 light source was used with an incidence angle of 10°. The three parameters L* (luminance on a scale of 0–100), a* (on a scale of redness to greenness) and b* (on a scale of yellowness to blueness) were determined based on X, Y and Z tristimulus values (Billmeyer & Saltzman, 1981; Christidis & Scott, 1997).

Results

Morphological characterization

The SEM images of BTT6 and BTT7 are presented in Fig. 3. The talc particles present a characteristic lamellar shape with particle

https://doi.org/10.1180/clm.2019.30 Published online by Cambridge University Press

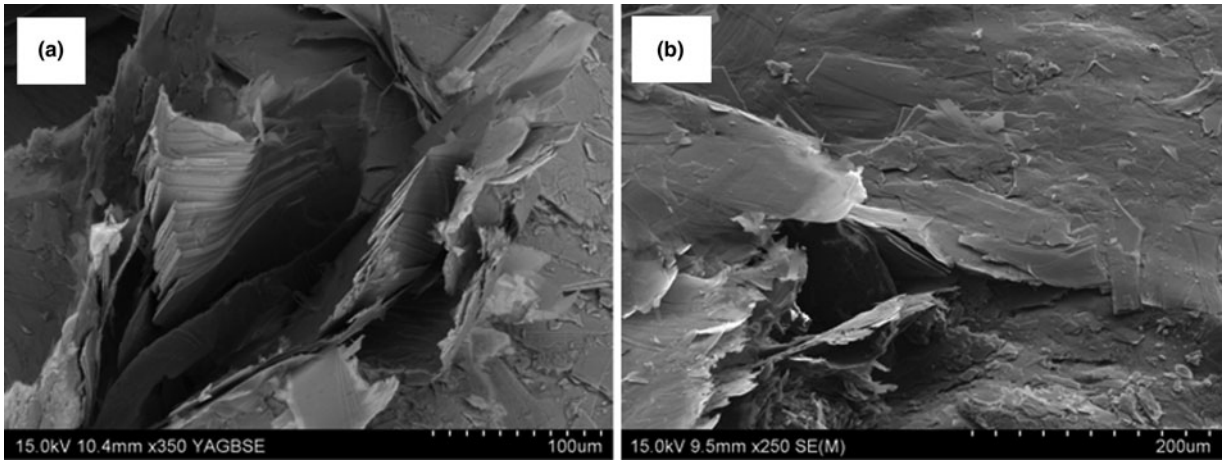

Fig. 3. SEM images of (a) BTT6 and (b) BTT7.

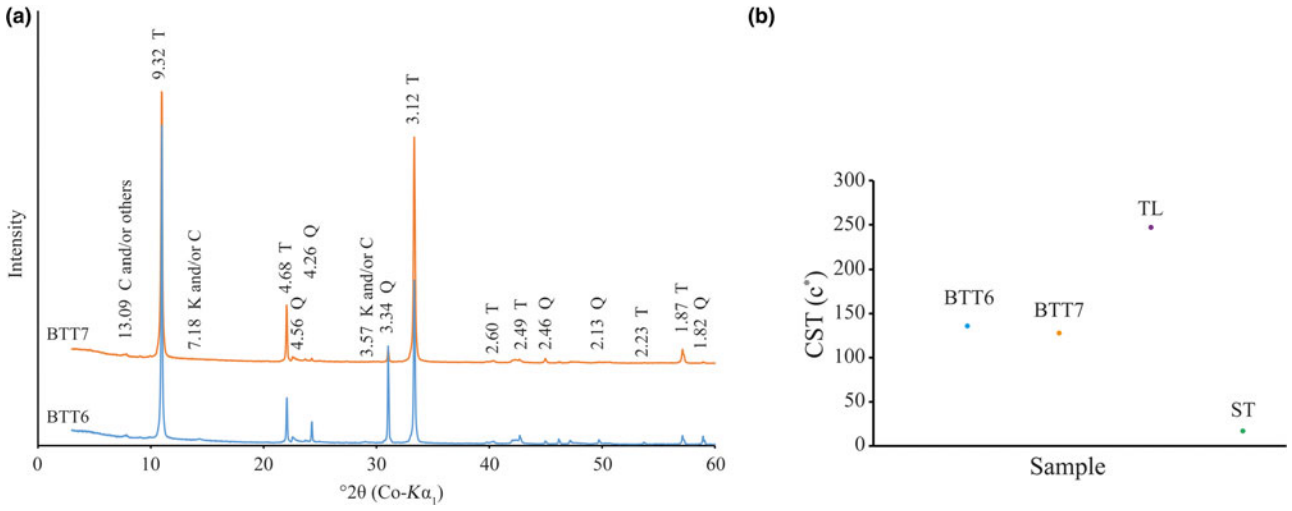

Fig. 4. (a) XRD traces of the coarse fraction (<250 μm; T = talc; Q = quartz; K = kaolinite; C = chlorite) of samples BTT6 and BTT7. (b) Crystal size thickness (CST) expressed in number of stacked layers of the BTT samples compared to the natural talc of Luzenac (TL) and a synthetic talc (ST).

sizes >100 μm. The lamellar morphology allows particle stacking along the c* axis through Van der Waals interactions (Alcover & Giese, 1986). This weak packing cohesion leads to partial exfoliation favouring delamination under grinding (Fig. 3a).

Mineralogical characterization

X-ray diffraction

The XRD traces of the BTT samples are shown in Fig. 4a (Boulingui, 2015). Talc is present in the samples, with typical *d* spacings at 9.32 Å (001), 4.68 Å (002) and 3.12 Å (003) (Brindley & Brown, 1980). Quartz is also present in both samples, being more abundant in BTT6 than in BTT7 based on the intensity of the diffraction lines. Finally, two small peaks at 13.09 and 7.18 Å reveal traces of chlorite and/or kaolinite, respectively. For chlorite, the 13.09 Å *d* spacing may indicate the presence of Fe and other substitutions in the lattice (Brindley & Gillery, 1956), but the presence of Al–Fe oxyhydroxide interlayers is not excluded. Identification of the Al–Fe-bearing phases is ambiguous because of the very small amounts present in the samples. The BTT6 and BTT7 samples were ground to ∼40 and ∼20 μm, respectively, with a mixer mill to avoid orientation effects and to intensify the signals of the accessory minerals.

The particle size distribution and XRD results are presented in Fig. 5a,b. The two samples contain comparable amounts of quartz. The bulk mineralogy remains unchanged, with the samples containing talc, quartz and traces of Al–Fe-bearing phases. The identification of the Al–Fe-bearing phases was also difficult after grinding because the main diffraction maxima of these phases did not increase. Although the peak at 13.09 Å disappeared after excessive grinding, the samples contain chlorite because the (002) reflection occurs at the same position as the (001) reflection of kaolinite (7.19 Å). It is suggested that the Al–Fe-bearing phase may be kaolinite, chlorite, Al–Fe oxyhydroxides and/or interstratified phase. The extremely small proportion of these phases makes it difficult to identify them conclusively.

The analysis of the full width at half maximum (FWHM) of the talc diffraction lines enabled estimation of crystal size from the coherent scattering thickness of the talc particles along the c* axis of the two samples with the Scherrer equation (Scherrer, 1918). BTT6 and BTT7 are composed of 136 and 128 stacked layers, respectively, crystallized perfectly along the c* direction

https://doi.org/10.1180/clm.2019.30 Published online by Cambridge University Press

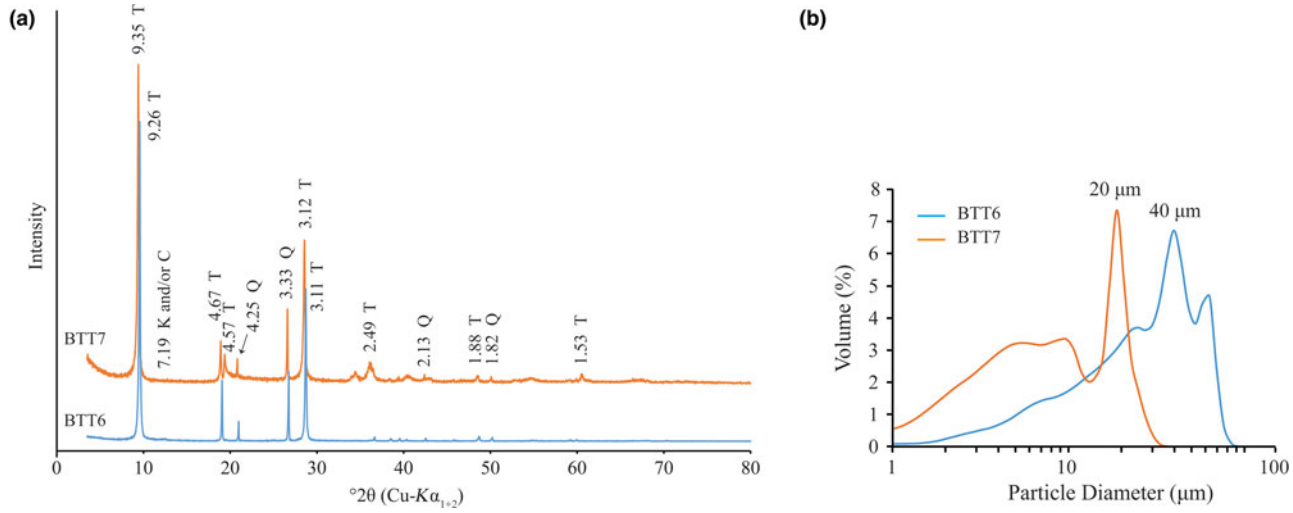

Fig. 5. (a) XRD traces (T = talc; Q = quartz; K = kaolinite; C = chlorite) and (b) particle-size distribution recorded on the fine fractions of BTT6 and BTT7.

Table 1. Modal composition of the BTT samples (Njopwouo, 1984; Boulingui, 2015).

Sample	Minerals	Theoretical chemical formula	Mass content (%)	Total (%)
BTT6	Talc	$Si_4Mg_3O_{10}(OH)_2$	66.2	99.5
	Quartz	SiO_2	29.3	
	Kaolinite, chlorite and/or Al–Fe oxyhydroxides	$Al_2Si_2O_5(OH)_4$ $Mg(Fe)_5Al_2Si_3O_{10}(OH)_8$ FeO(OH), AlO(OH)	4.0	
	Others			0.5
BTT7	Talc	$Si_4Mg_3O_{10}(OH)_2$	89.2	98.4
	Quartz	SiO_2	7.9	
	Kaolinite, chlorite and/or Al–Fe oxyhydroxides	$Al_2Si_2O_5(OH)_4$ $Mg(Fe)_5Al_2Si_3O_{10}(OH)_8$ FeO(OH), AlO(OH)	1.3	
	Others			1.6

(Fig. 4b). These values correspond to a talc of intermediate crystal order in comparison with a well-crystallized natural talc (247 stacked layers, Trimouns quarry, Luzenac, France) or a poorly crystallized synthetic talc (10 stacked layers; Dumas *et al.*, 2016).

Weight content calculations

Modal compositions enabled the establishment of the percentage of each phase in the samples (Yvon *et al.*, 1990). The method has been used extensively in the past (Njoya *et al.*, 2006; Nkoumbou *et al.*, 2006; Boulingui *et al.*, 2015). Sample BTT7 is very pure mineralogically as it contains 90.0 wt.% talc, with minor quartz (7.9 wt.%) and trace Al–Fe-bearing phases (1.3 wt.%) (Table 1). Sample BTT6 contains only 66.0 wt.% of talc with a higher proportion of quartz (29.0 wt.%) and Al–Fe-bearing phases (4.0 wt.%). This outcome should be correlated generally to the XRD results, but some variations may exist because of experimental factors, such as the mineralogy of the analysed fraction or the mineral orientation during the XRD analysis.

Chemical characterization

Whole-rock chemical analysis

The whole-rock chemical results are in good agreement with the XRD data (Table 2). Indeed, BTT6 and BTT7 exhibit an excess of SiO_2 related to the presence of quartz in both samples. Sample BTT6 is richer in SiO_2, in accord with the greater amount of quartz in the sample. The samples also contain small amounts of Al_2O_3 (<1 wt.%; Table 2) and traces of Fe_2O_3 related to the trace presence of Al–Fe-bearing phases in the samples. The SiO_2/MgO ratio of BTT7 is very close to the theoretical composition of talc (Ersoy *et al.*, 2013). This highlights the greater mineralogical purity of this sample compared to BTT6. Finally, the values obtained for trace elements (Table 3) show high proportions of lithophile (Ce), chalcophile (Zn) and siderophile elements (Cr, V).

Table 2. Bulk chemical composition (wt.%) of the BTT samples (major elements).

Compound	BTT6	BTT7	Theoretical value for a pure talc
SiO_2	72.59	64.93	63.5
Al_2O_3	0.77	0.34	0
Fe_2O_3	0.20	0.05	0
MnO	0.00	0.00	0
MgO	21.80	28.65	31.7
CaO	0.04	<LD	0
Na_2O	0.08	0.11	0
K_2O	0.01	0.01	0
TiO_2	0.03	<LD	0
P_2O_5	<LD	<LD	0
L.O.I.	4.33	5.17	4.8
Total	99.85	99.25	100

<LD = below limit of detection; LOI = loss on ignition at 1050°C.

https://doi.org/10.1180/clm.2019.30 Published online by Cambridge University Press

Table 3. Bulk minor and trace element compositions (ppm) of the BTT samples.

Element	BTT6	BTT7
As	<LD	<LD
Ba	3.935	2.783
Be	<LD	<LD
Bi	<LD	<LD
Cd	<LD	<LD
Ce	8.950	0.370
Co	0.351	0.218
Cr	20.420	13.440
Cs	<LD	<LD
Cu	<LD	<LD
Dy	0.590	0.319
Er	0.302	0.207
Eu	0.186	0.076
Ga	0.954	0.209
Gd	0.776	0.333
Ge	<LD	<LD
Hf	0.148	0.053
Ho	0.111	0.070
In	<LD	<LD
La	5.751	0.952
Lu	0.044	0.039
Mo	<LD	<LD
Nb	0.482	0.140
Nd	5.658	1.535
Ni	<LD	<LD
Pb	1.784	<LD
Pr	1.425	0.331
Rb	0.410	<LD
Sc	1.230	<LD
Sb	<LD	<LD
Sm	1.008	0.364
Sn	<LD	<LD
Sr	<LD	<LD
Ta	0.042	0.010
Tb	0.107	0.051
Th	0.486	0.153
Tm	0.046	0.032
U	0.307	0.159
V	8.921	6.641
W	0.520	0.363
Y	3.242	1.929
Yb	0.291	0.235
Zn	11.370	<LD
Zr	5.691	2.010

<LD = below limit of detection.

Talc crystal chemistry

Microprobe analyses of the pressed powder pellets of samples BTT6 and BTT7 (Table 4) showed that the SiO_2/MgO wt.% ratios (R) were 2.22 and 2.09 in BTT6 and BTT7, respectively, with the latter being very close to $R = 2.00$ (*i.e.* the theoretical talc composition; Ersoy *et al.*, 2013). Therefore, the microprobe analysis recorded the chemical composition of the talc particles rather than the bulk composition due to the preferential orientation of the talc particles along their *ab* plane, concealing at the same time the mineral impurities present in smaller quantities in the samples. Moreover, all of the measurements were focused on large talc particles to avoid the analysis of accessory minerals. On this basis, it is reasonable to assume that the remaining metal oxides recorded in the analysis (*e.g.* Fe_2O_3) originate from the talc crystal lattice rather than from impurities (Al–Fe-bearing phases). Indeed, Fe atoms may substitute for Si or Mg atoms located in the tetrahedral and octahedral sheets of sheet silicates (Martin *et al.*, 1999). This was particularly demonstrated by Petit *et al.* (2004), who revealed the presence of Fe substitutions in the crystal lattices of 15 natural talcs. Among them, the talc of Luzenac, which corresponds to our natural talc of reference, contains 0.68 wt.% Fe_2O_3 in its crystal lattice. This amount is much greater than those obtained in the talcs from Gabon (0.16 wt.% for BTT6 and 0.04 wt.% for BTT7). Hence, the talcs of Minzanzala are chemically very pure despite their association with other mineral impurities in the samples.

Table 4. Electron microprobe analyses and structural formulae of the talc particles.

Compound	BTT6	BTT7	Theoretical value
Wt.%			
SiO_2	64.72	64.00	63.5
Na_2O	0.09	0.09	
Al_2O_3	0.97	0.23	
Fe_2O_3	0.16	0.04	
CaO	0.01	0.01	
MgO	29.13	30.62	31.7
Cl	0.01	0.01	
F	1.41	1.44	
H_2O	4.01	3.98	4.8
O = F, Cl	0.60	0.61	
Total	99.89	99.79	100
Structural formulae of talc based on 22 oxygen equivalents			
Si	8.22	8.16	8.00
Na	0.02	0.02	
Al	0.15	0.03	
Fe	0.02	0.01	
Ca	0.00	0.00	
Mg	5.58	5.89	6.00
Cl	0.00	0.00	
F	0.57	0.59	
OH	3.42	3.43	4.00

In addition, F is present in relatively high proportions in the two talc samples (1.41 wt.% in BTT6 and 1.44 wt.% in BTT7). This F content is in the average range of those observed for other talc samples coming from various parts of the world (Petit *et al.*, 2004), and its presence is characteristic of natural environments in which the F atoms can substitute for the OH groups, pointing towards the hexagonal cavities of Si tetrahedra (Ross & Smith, 1968; Abercrombie *et al.*, 1987). It is suggested that this F is not derived from other mineral phases because the microprobe analysis was specifically focused on large talc platelets, as noted above.

Crystal-chemical characterization

Talc particles

The ^{29}Si and ^{1}H NMR spectra enabled the evaluation of the crystal-chemistry of the two talc samples and permitted the determination of the possible Fe substitutions in the crystal lattice by measuring the FWHM of the main NMR peaks. A talc with large amounts of Fe substitutions exhibits wide peaks in the ^{1}H and ^{29}Si MAS-NMR spectra, whereas a chemically very pure talc will exhibit narrow peaks (Martin *et al.*, 2006).

In our case, the ^{29}Si MAS-NMR spectra of BTT6 and BTT7 are composed of a symmetrical narrow peak at ~ –98 ppm, attributed to Q^3 species (Lippmaa *et al.*, 1980) (Fig. 6a), which indicates that the samples are very pure chemically. This assumption was validated by comparing their spectra with that of the Luzenac talc, which contains more Fe substitutions. The differences in the FWHM between the three samples clearly demonstrate the chemical purity of the talcs of Minzanzala (Fig. 6b), which is in full

https://doi.org/10.1180/clm.2019.30 Published online by Cambridge University Press

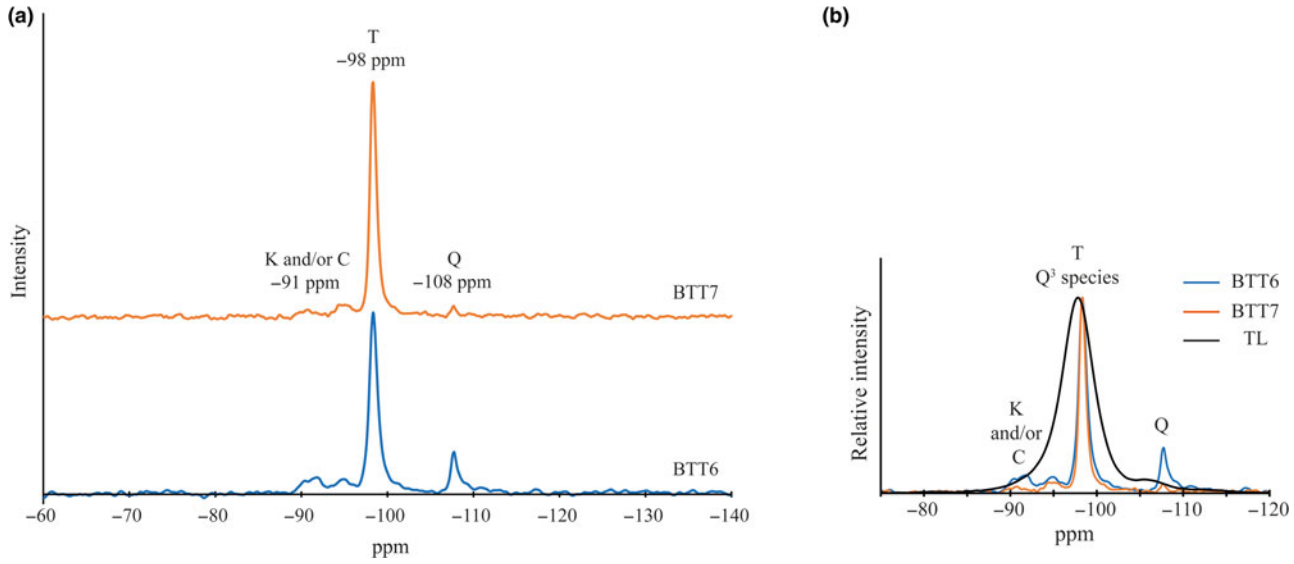

Fig. 6. (a) Solid-state ^{29}Si MAS-NMR spectra of BTT6 and BTT7 (T = talc; Q = quartz; K = kaolinite; C = chlorite) and (b) comparison with the natural talc of Luzenac (TL).

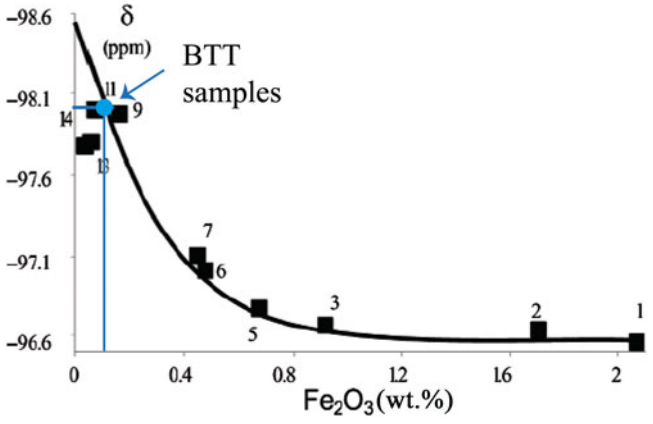

Fig. 7. Chemical shift (δ) *vs.* Fe_2O_3 diagram, allowing the estimation of the Fe_2O_3 content of the BTT samples (according to the correlation line of Martin *et al.*, 2006).

agreement with the microprobe analysis. Martin *et al.* (2006) demonstrated that the position of this same peak can be correlated to the amount of Fe_2O_3 present in the sample. Projection of the –98 ppm position in a correlation line (Fig. 7) shows that the two samples have very low Fe_2O_3 contents (~0.1 wt.%), which is also in agreement with the microprobe results. The ^{29}Si MAS-NMR spectra also provided evidence of a potential small fraction of nano-sized talc particles in the samples located at –95 ppm. This resonance has been attributed to nano-sized synthetic talc particles (Dumas *et al.*, 2016) rather than quartz, kaolinite or chlorite because their ^{29}Si chemical shifts are located elsewhere (–108 ppm for quartz; –91 ppm for kaolinite and chlorite).

The chemical purity of BTT6 and BTT7 was also confirmed by the ^{1}H MAS-NMR spectra (Fig. 8a). The samples display a major symmetrical peak at 0.8 ppm corresponding to H atoms located within the hexagonal cavities of the talc structure (Martin *et al.*, 2006). The narrowness of this peak indicates that the talcs are chemically very pure, otherwise their FWHM would be greater. The comparison of the ^{1}H NMR spectra of BTT6 and BTT7 with the talc of Luzenac (rich in Fe substitutions) confirmed once again the chemical purity of the Gabonese talc (Fig. 8b). Finally, the presence of the smaller peak at 4.7 ppm in the ^{1}H MAS-NMR spectra of the two samples demonstrates the presence of residual physisorbed water on the talc particle edges (Dumas *et al.*, 2013).

The NIR spectra of BTT6 and BTT7 are shown in Fig. 9a. Small amounts of of Fe substitutions yield bands at 7156 cm^{-1} ($2\upsilon Mg_2FeOH$), 7118 cm^{-1} ($2\upsilon MgFe_2OH$) and 7073 cm^{-1} ($2\upsilon Fe_3OH$) (Petit *et al.*, 2004). In the present study, these bands are absent from the NIR spectra, corroborating the very good chemical purity of the talcs (Fig. 9b), which is in agreement with the previous microprobe and MAS-NMR results. The band at 5240 cm^{-1} (Fig. 9a) confirms the presence of physisorbed water on the talc particle edges (Dumas *et al.*, 2013). In summary, the NIR spectra of the Minzanzala talcs show the typical vibration bands of a very pure talc structure, with major bands located at 7184 cm^{-1} for the $2\upsilon Mg_3OH$ vibration and at 4051, 4180, 4323 and 4367 cm^{-1} for the OH combination bands (Zhang *et al.*, 2006).

Evidence for accessory minerals

The presence of accessory minerals was examined by ^{29}Si MAS-NMR and NIR spectroscopies (Figs 6a, 9b). The peak of low intensity at –91 ppm in the ^{29}Si MAS-NMR spectra indicates the presence of kaolinite and/or chlorite in the two samples (Massiot *et al.*, 1995; Zazzi *et al.*, 2006). This observation is supported by the weak band at 7065 cm^{-1} in the NIR spectra, attributed to the $2\upsilon Al_2OH$ vibration of kaolinite (Petit *et al.*, 1999). In addition, the band at 4525 cm^{-1} corresponds to the combination of the $2\delta Al_2OH$ and $2\upsilon Al_2OH$ vibrations of kaolinite and/or chlorite (Yang *et al.*, 2018). The presence of chlorite might be verified by the presence of two diagnostic bands at 4280 and 4440 cm^{-1}. In the present study, these bands are absent, suggesting that chlorite might not exist in the Minzanzala samples. Nevertheless, the presence of chlorite should not be excluded because of the existence of the peak at 13.09 Å in the XRD traces. Obviously, the Minzanzala talc samples do contain some traces of kaolinite, but the presence of chlorite is questionable and may vary from one sample to another.

https://doi.org/10.1180/clm.2019.30 Published online by Cambridge University Press

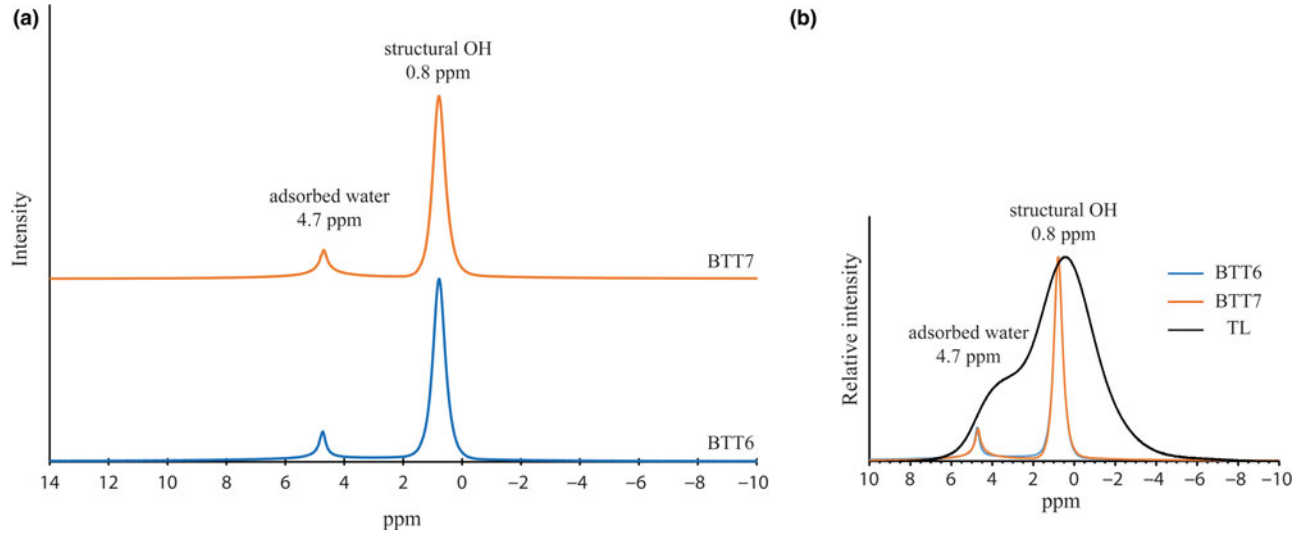

Fig. 8. (a) Solid-state ^{1}H MAS-NMR spectra of BTT6 and BTT7 and (b) comparison with the natural talc of Luzenac (TL).

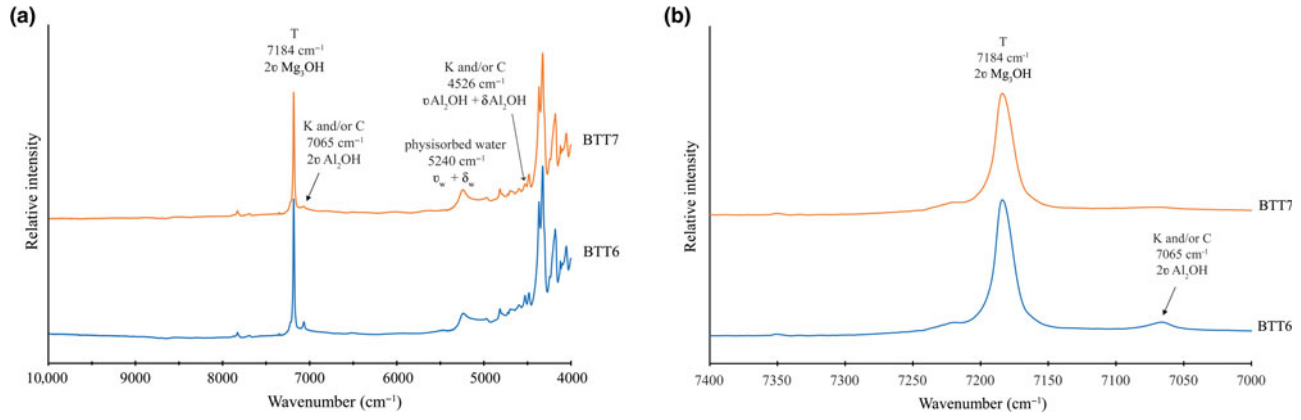

Fig. 9. (a) NIR spectra recorded on BTT6 and BTT7 samples (T = talc; K = kaolinite; C = chlorite) and (b) enhancement of the 7000–7400 cm^{-1} range, confirming the absence of Fe substitution in the talc crystal lattice.

The presence of quartz was indicated by a thin peak at −108 ppm on the ^{29}Si MAS-NMR spectra of the two samples. Comparison of the peak areas in BTT6 and BTT7 confirms that BTT6 is richer in accessory minerals (quartz, Al–Fe-bearing phases) than BTT7.

Table 5. Colour properties of the talc samples from Gabon.

Sample	L*	a*	b*
BTT6	90.51	1.05	12.15
BTT7	94.78	0.59	5.65

Colour properties

Table 5 lists the colour properties of the two Gabonese talcs. The talcs are white (high L* values) with a low red hue (a* parameter). They nevertheless present a yellowish hue according to the higher b* parameter values. This value is more significant for BTT6, which confirms the observations made with the naked eye. The colour might be attributed to the presence of accessory chlorite or to traces of Fe oxyhydroxides.

Potential applications

The remarkable chemical purity of the talc particles combined with the small percentage of accessory minerals in the deposit (especially for BTT7) suggest applications in cosmetics. The cosmetics industry requires talc deposits of very high quality, as up to 90% should be composed of talc and should be free of fibrous or asbestos-form minerals (Fiume *et al.*, 2015). The talc particles should also have very low Pb (<20 ppm) and As contents (<3 ppm), and they should be free of quartz. When looking at these specifications (cf. Tables 1, 3), the BTT7 sample satisfies these requirements except for the presence of quartz in the sample. Nevertheless, quartz may be removed easily by flotation (use of pine oil as a frother) or by mechanical processes (*i.e.* cyclonic sedimentation). Moreover, if necessary, acid leaching may be used to remove impurities such as CaO, Fe_2O_3 or Al_2O_3 (Barani & Aghazadeh, 2018). Based on these results, the Minzanzala talc ore is a potential candidate for supplying cosmetic talc to the global market.

https://doi.org/10.1180/clm.2019.30 Published online by Cambridge University Press

In addition, the Gabonese talcs might be used in the ceramic or paint industries to produce catalytic converters or matte paints (even if the quartz fraction is not removed). Moreover, they might be employed as fillers in hydrophobic polymers for enhancing the mechanical and thermal properties of the composites. In this case, the particle size should be reduced by milling to enhance the dispersion of the talc particles in the polymers (Yousfi *et al.*, 2013). In contrast, the Minzanzala talcs may be less appropriate for the paper and white ceramic industries (primarily BTT6) because of their yellowish hue and mineral impurities, which would tarnish the sought-after whiteness of the products.

Conclusions

Two talc samples from the Minzanzala deposit of Gabon were characterized in order to determine their crystal-chemistry and mineralogy. The samples contain quartz and Al–Fe-bearing phase impurities (kaolinite, chlorite and/or Al–Fe oxyhydroxides) in comparable proportions. However, despite the presence of impurities, the talc particles have high chemical quality, as was determined by several analytical methods (microprobe analysis, ^{1}H and ^{29}Si MAS-NMR spectroscopy and NIR spectroscopy) that provided evidence of a very small Fe content in the talc lattice. Finally, colour measurements demonstrated a yellowish hue in both samples, which is probably related to the presence of chlorite and/or Al–Fe oxyhydroxides. It is suggested that the talc deposit of Minzanzala could be used in several applications, especially in cosmetics, paints, polymers and ceramics (production of catalytic converters) due to its high chemical quality. However, some applications should be avoided (papers and white ceramics) because of their yellowish hue (especially BTT6) and the presence of other mineral phases, which might affect the whiteness of the final product. Finally, special attention should be paid to the presence of significant amounts of quartz, which would increase the abrasiveness of the end product.

Author ORCIDs. M. Poirier, 0000-0001-7917-2080.

Acknowledgements. The authors thank the Ecole Normale Supérieure of Libreville (Gabon) and the Université de Lorraine (France) for their support and of this work. They also thank Christel Carême for the colorimetry measurements (Imerys, France) and Philippe de Parseval for the microprobe analysis (Centre de MicroCaractérisation Raimond Castaing, Toulouse, France).

References

Abercrombie H.J., Skippen G.B. & Marshall D.D. (1987) F–OH substitution in natural tremolite, talc, and phlogopite. *Contributions to Mineralogy and Petrology*, **97**, 305–312.

Alcover J.F. & Giese R.F. (1986) Energie de liaison des feuillets de talc, pyrophyllite, muscovite et phlogopite. *Clay Minerals*, **21**, 159–169.

Barani K. & Aghazadeh V. (2018) Removal of impurities from talc ore by leaching method. *Journal of Chemical Technology and Metallurgy*, **53**, 296–300.

Bellivier F. (1977) *Prospection de talc dans la région de Ndendé*. Bureau de Recherches Géologiques et Minières, Orléans, France.

Billmeyer F.W. & Saltzman M. (1981) *Principles of Color Technology*, 2nd edn. Wiley-Interscience, New York, NY, USA.

Boulingui J.-E. (2015) *Inventaire des ressources en argiles du Gabon et leurs utilisations conventionnelles ou non dans les régions de Libreville de Tchibanga*. Doctoral thesis. Université de Lorraine, Nancy, France, and Université de Yaoundé, Yaoundé, Cameroon.

Boulingui J.E., Nkoumbou C., Njoya D., Thomas F. & Yvon J. (2015) Characterization of clays from Mezafe and Mengono (NE-Libreville, Gabon) for potential uses in fired products. *Applied Clay Science*, **115**, 132–144.

Boutin P. (1985) *Talc du synclinal de la Nyanga (Gabon). Synthèse des travaux fin 1984*. Bureau de Recherches Géologiques et Minières, Orléans, France.

Boutin P., Récoché G., Perrin J., Spencer C. & Bouchot V. (2001) *Développement et mise en valeur des ressources naturelles de la province de la Nyanga (Gabon) – Programme de promotion des ressources minérales du synclinal de la Nyanga*. Bureau de Recherches Géologiques et Minières, Orléans, France.

Brindley G.W. & Brown G. (1980) *Crystal Structures of Clay Minerals and Their X-Ray Identification*. Mineralogical Society, London, UK.

Brindley G. & Gillery F. (1956) X-ray identification of chlorite species. *American Mineralogist*, **41**, 169–186.

Carretero M.I. & Pozo M. (2010) Clay and non-clay minerals in the pharmaceutical and cosmetic industries Part II. Active ingredients. *Applied Clay Science*, **47**, 171–181.

Chandra N., Agnihotri N. & Bhasin S.K. (2004) Sintering characteristics of talc in the presence of phosphatic and alkali carbonate sintering activators. *Ceramics International*, **30**, 643–652.

Chauhan V.S. & Bhardwaj N.K. (2017) Efficacy of dispersion of magnesium silicate (talc) in papermaking. *Arabian Journal of Chemistry*, **10**, S1059–S1066.

Christidis G.E. & Scott P.W. (1997) Origin and colour properties of white bentonite: a case study from the Aegean Islands of Milos and Kimolos, Greece. *Mineralium Deposita*, **32**, 271–279.

Dumas A. (2013) *Elaboration de nouveaux procédés de synthèse et caractérisation de talcs sub-microniques: de la recherche fondamentale vers des applications industrielles*. PhD thesis. Université Toulouse III – Paul Sabatier, Toulouse, France.

Dumas A., Martin F., Le Roux C., Micoud P., Petit S., Ferrage E., Brendlé J., Grauby O. & Greenhill-Hooper M. (2013) Phyllosilicates synthesis: a way of accessing edges contributions in NMR and FTIR spectroscopies. Example of synthetic talc. *Physics and Chemistry of Minerals*, **40**, 361–373.

Dumas A., Martin F., Ngo Ke T., Nguyen Van H., Nguyen Viet D., Nguyen Tat V., Kieu Quy N., Micoud P. & de Parseval P. (2015) The crystal-chemistry of Vietnamese talcs from the Thanh Son district (Phu Tho province, Vietnam). *Clay Minerals*, **50**, 607–617.

Dumas A., Claverie M., Slostowski C., Aubert G., Careme C., Le Roux C., Micoud P., Martin F. & Aymonier C. (2016) Fast-geomimicking using chemistry in supercritical water. *Angewandte Chemie International Edition*, **55**, 9868–9871.

Ersoy B., Dikmen S., Yildiz A., Gören R. & Elitok Ö. (2013) Mineralogical and physicochemical properties of talc from Emirdağ, Afyonkarahisar, Turkey. *Turkish Journal of Earth Sciences*, **22**, 632–644.

Fiume M.M., Boyer I., Bergfeld W.F., Belsito D.V., Hill R.A., Klaassen C.D., Liebler D.C., Marks J.G., Shank R.C., Slaga T.J., Snyder P.W. & Andersen F.A. (2015) Safety assessment of talc as used in cosmetics. *International Journal of Toxicology*, **34**, 66S–129S.

Kocic N., Kretschmer K., Bastian M. & Heidemeyer P. (2012) The influence of talc as a nucleation agent on the nonisothermal crystallization and morphology of isotactic polypropylene: the application of the Lauritzen–Hoffmann, Avrami, and Ozawa theories. *Journal of Applied Polymer Science*, **126**, 1207–1217.

Lippmaa E., Mägi M., Samoson A., Engelhardt G. & Grimmer A.R. (1980) Structural studies of silicates by solid-state high-resolution silicon-29 NMR. *Journal of the American Chemical Society*, **102**, 4889–4893.

Lissoulour X. & Barras X. (1948) *Prospection de la région de la Nyanga et de la basse Nyanga Group VII*. Document COGEMA-CEA 48 GAB RSP-3. Commissariat à l'Energie Atomique, Paris, France.

López-Galindo A., Viseras C. & Cerezo P. (2007) Compositional, technical and safety specifications of clays to be used as pharmaceutical and cosmetic products. *Applied Clay Science*, **36**, 51–63.

Mallet S., Delord P., Juin H. & Lessire M. (2005) Effect of feed in talc supplementation on broiler performance. *Animal Research*, **54**, 485–492.

Martin F., Micoud P., Delmotte L., Marichal C., Le Dred R., de Parseval P., Mari A., Fortuné J.P., Salvi S. & Béziat D. (1999) The structural formula of talc from the Trimouns deposit, Pyrénées, France. *The Canadian Mineralogist*, **37**, 997–1006.

https://doi.org/10.1180/clm.2019.30 Published online by Cambridge University Press

Martin F., Ferrage E., Petit S., de Parseval P., Delmotte L., Ferret J., Arseguel D. & Salvi S. (2006) Fine-probing the crystal-chemistry of talc by MAS-NMR spectroscopy. *European Journal of Mineralogy*, **18**, 641–651.

Martini J. & Makanga J.F. (2001) *Carte métallogénique de la République Gabonaise*. Council for Geoscience, Pretoria, South Africa.

Maskell N.A., Lee Y.C.G., Gleeson F.V., Hedley E.L., Pengelly G. & Davies R.J.O. (2004) Randomized trials describing lung inflammation after pleurodesis with talc of varying particle size. *American Journal of Respiratory and Critical Care Medicine*, **170**, 377–382.

Massiot D., Dion P., Alcover J.F. & Bergaya F. (1995) ^{27}Al and ^{29}Si NMR study of kaolinite thermal decomposition by controlled rate thermal analysis. *Journal of the American Ceramic Society*, **78**, 2940–2944.

Müller A., Breiter K., Seltmann R. & Pécskay Z. (2005) Quartz and feldspar zoning in the eastern Erzgebirge volcano–plutonic complex (Germany, Czech Republic): evidence of multiple magma mixing. *Lithos*, **80**, 201–227.

Njopwouo D. (1984) *Minéralogie et physico-chimie des argiles de Bomkoul et de Balengou (Cameroun). Utilisation dans la polymérisation du styrène et dans le renforcement du caoutchouc naturel*. Doctoral thesis, Université de Yaoundé, Yaoundé, Cameroon.

Njoya A., Nkoumbou C., Grosbois C., Njopwouo D., Njoya D., Courtinnomade A., Yvon J. & Martin F. (2006) Genesis of Mayouom kaolin deposit (western Cameroon). *Applied Clay Science*, **32**, 125–140.

Nkoumbou C., Njopwouo D., Villiéras F., Njoya A., Yonta Ngouné C., Ngo Ndjock L., Tchoua F.M. & Yvon J. (2006) Talc indices from Boumnyebel (central Cameroon), physico-chemical characteristics and geochemistry. *Journal of African Earth Sciences*, **45**, 61–73.

Petit S., Madejová J., Decarreau A. & Martin F. (1999) Characterization of octahedral substitutions in kaolinites using near infrared spectroscopy. *Clays and Clay Minerals*, **47**, 103–108.

Petit S., Martin F., Wiewiora A., de Parseval P. & Decarreau A. (2004) Crystal-chemistry of talc: a near infrared (NIR) spectroscopy study. *American Mineralogist*, **89**, 319–326.

Ross M. & Smith W.L. (1968) Triclinic talc and associated amphiboles from Gouverneur Mining District, New York. *American Mineralogist*, **53**, 751–769.

Scherrer P. (1918) Bestimmung der grösse und der inneren struktur von kolloidteilchen mittels Röntgenstrahlen, Nachr. *Gesellschaft für Wissenschaftliche zu Göttingen*, **26**, 98–100.

Tothill I.E., Best D.J. & Seal K.J. (1993) Studies on the inhibitory effect of paint raw materials on cellulolytic enzymes present in waterborne paint. *International Biodeterioration and Biodegradation*, **32**, 233–242.

Viallat J.R. & Boutin C. (1998) Épanchements pleuraux malins: le recours précoce au talcage. *La Revue de Médecine Interne*, **19**, 811–818.

Yang M., Ye M., Han H., Ren G., Han L. & Zhang Z. (2018) Near-infrared spectroscopic study of chlorite minerals. *Journal of Spectroscopy*, **2018**, 6958260.

Yousfi M., Livi S., Dumas A., Le Roux C., Crépin-Leblond J., Greenhill-Hooper M. & Duchet-Rumeau J. (2013) Use of new synthetic talc as reinforcing nanofillers for polypropylene and polyamide 6 systems: thermal and mechanical properties. *Journal of Colloid and Interface Science*, **403**, 29–42.

Yvon J., Baudracco J., Cases J.M. & Weiss J. (1990) Eléments de minéralogie quantitative en micro-analyse des argiles. Pp. 473–489 in: *Matériaux Argileux, Structures, Propriétés et Applications* (A. Decarreau, editor). Société Française de Minéralogie et de Cristallographie–Groupe Français des Argiles, Paris, France.

Zazenski R., Ashton W.H., Briggs D., Chudkowski M., Kelse J.W., MacEachern L., McCarthy E.F., Nordhauser M.A., Roddy M.T., Teetsel N.M., Wells A.B. & Gettings S.D. (1995) Talc: occurrence, characterization, and consumer applications. *Regulatory Toxicology and Pharmacology*, **21**, 218–229.

Zazzi Å., Hirsch T.K., Leonova E., Kaikkonen A., Grins J., Annersten H. & Edén M. (2006) Structural investigations of natural and synthetic chlorite minerals by X-ray diffraction, Mössbauer spectroscopy and solid-state nuclear magnetic resonance. *Clays and Clay Minerals*, **54**, 252–265.

Zhang M., Hui Q., Lou X.-J., Redfern S.A.T., Salje E.K.H. & Tarantino S. (2006) Dehydroxylation, proton migration, and structural changes in heated talc: an infrared spectroscopic study. *American Mineralogist*, **91**, 816–825.

https://doi.org/10.1180/clm.2019.30 Published online by Cambridge University Press